AAV8BP2 and AAV8 transduce the mammalian cochlear lateral wall and endolymphatic sac with high efficiency

Kevin Isgrig,[1,6] Yasuko Ishibashi,[1,6] Hyun Jae Lee,[2] Jianliang Zhu,[1] Mhamed Grati,[1] Jean Bennett,[3] Andrew J. Griffith,[2,4] Isabelle Roux,[2] and Wade W. Chien[1,5]

[1]Inner Ear Gene Therapy Program, National Institute on Deafness and Other Communication Disorders (NIDCD), National Institutes of Health, Bethesda, MD, USA; [2]Otolaryngology Branch, NIDCD, National Institutes of Health, Bethesda, MD, USA; [3]Center for Advanced Retinal and Ocular Therapeutics, University of Pennsylvania Perelman School of Medicine, Philadelphia, PA, USA; [4]Department of Otolaryngology, University of Tennessee College of Medicine, Memphis, TN, USA; [5]Department of Otolaryngology-Head and Neck Surgery, Johns Hopkins School of Medicine, Baltimore, MD, USA

Inner ear gene therapy using adeno-associated viruses (AAVs) has been successfully applied to several mouse models of hereditary hearing loss to improve their auditory function. While most inner ear gene therapy studies have focused on the mechanosensory hair cells and supporting cells in the organ of Corti, the cochlear lateral wall and the endolymphatic sac have not garnered much attention. The cochlear lateral wall and the endolymphatic sac play critical roles in inner ear ionic and fluid homeostasis. Mutations in genes expressed in the cochlear lateral wall and the endolymphatic sac are present in a large percentage of patients with hereditary hearing loss. In this study, we examine the transduction patterns and efficiencies of conventional (AAV2 and AAV8) and synthetic (AAV2.7m8, AAV8BP2, and Anc80L65) AAVs in the mouse inner ear. We found that AAV8BP2 and AAV8 are capable of transducing the marginal cells and intermediate cells in the stria vascularis. These two AAVs can also transduce the epithelial cells of the endolymphatic sac. Our data suggest that AAV8BP2 and AAV8 are highly useful viral vectors for gene therapy studies targeting the cochlear lateral wall and the endolymphatic sac.

INTRODUCTION

Adeno-associated virus (AAV) is one of the most commonly used viral vectors for gene therapy studies.[1] Over the past few years, several studies have shown that AAV-mediated gene therapy can be successfully applied to mouse models of hereditary hearing loss and dizziness to improve the auditory and vestibular functions in these animals.[2–17] While most studies on AAV-mediated inner ear gene delivery have focused on transducing the mechanosensory hair cells and non-sensory supporting cells in the organ of Corti, the cochlear lateral wall and endolymphatic sac have not garnered as much attention.[18] However, the cochlear lateral wall and the endolymphatic sac play critical roles in regulating the ionic and fluid transports in the inner ear, in order to maintain the volume and unique composition of the endolymph (e.g., high potassium [K$^+$] and low sodium [Na$^+$] ion concentrations) necessary for proper inner ear function. The cochlear lateral wall is located at the lateral border of the scala media. It consists of the stria vascularis, the spiral prominence, and the spiral ligament (Figure 1). The stria vascularis has three distinct cellular layers: marginal, intermediate, and basal cell layers. Marginal cells form a monolayer in the apical surface of the stria vascularis, and separate the endolymph from the intrastrial space (Figure 1, inset). The intermediate cells and basal cells occupy the basolateral side of the intrastrial space. K$^+$ ions are transported through the different layers of the stria vascularis by ion transporters, such as KCNJ10, SLC12A2, and KCNQ1/KCNE1, toward the endolymph.[19,20] Mutations in *KCNQ1/KCNE1* and *KCNJ10* are known causes of hereditary hearing loss (OMIM: 612347, 600791, and 612780). In addition to the stria vascularis, the fibrocytes in the spiral ligament and the root cells in the spiral prominence also contribute to K$^+$ recycling.[21,22] The cells in the cochlear lateral wall are connected to each other through an extensive gap junction network.[23,24] Mutations in the gap junction gene *GJB2* and deletions in the *GJB2-GJB6* genomic region are among the most common causes of hereditary hearing loss.[25–30]

The endolymphatic sac is a fluid-filled pouch that is part of the endolymphatic system. It plays an important role in ion transport and fluid absorption.[32,33] It is composed of a monolayer of epithelial cells composed of two main cell types classified by their appearance in transmission electron microscopy: ribosome-rich cells and mitochondria-rich cells.[34] Ribosome-rich cells have abundant ribosomes, rough endoplasmic reticulum, and a transcriptomic signature suggesting that they play an important role in the expression and secretion of extracellular proteins.[33] Mitochondria-rich cells are characterized
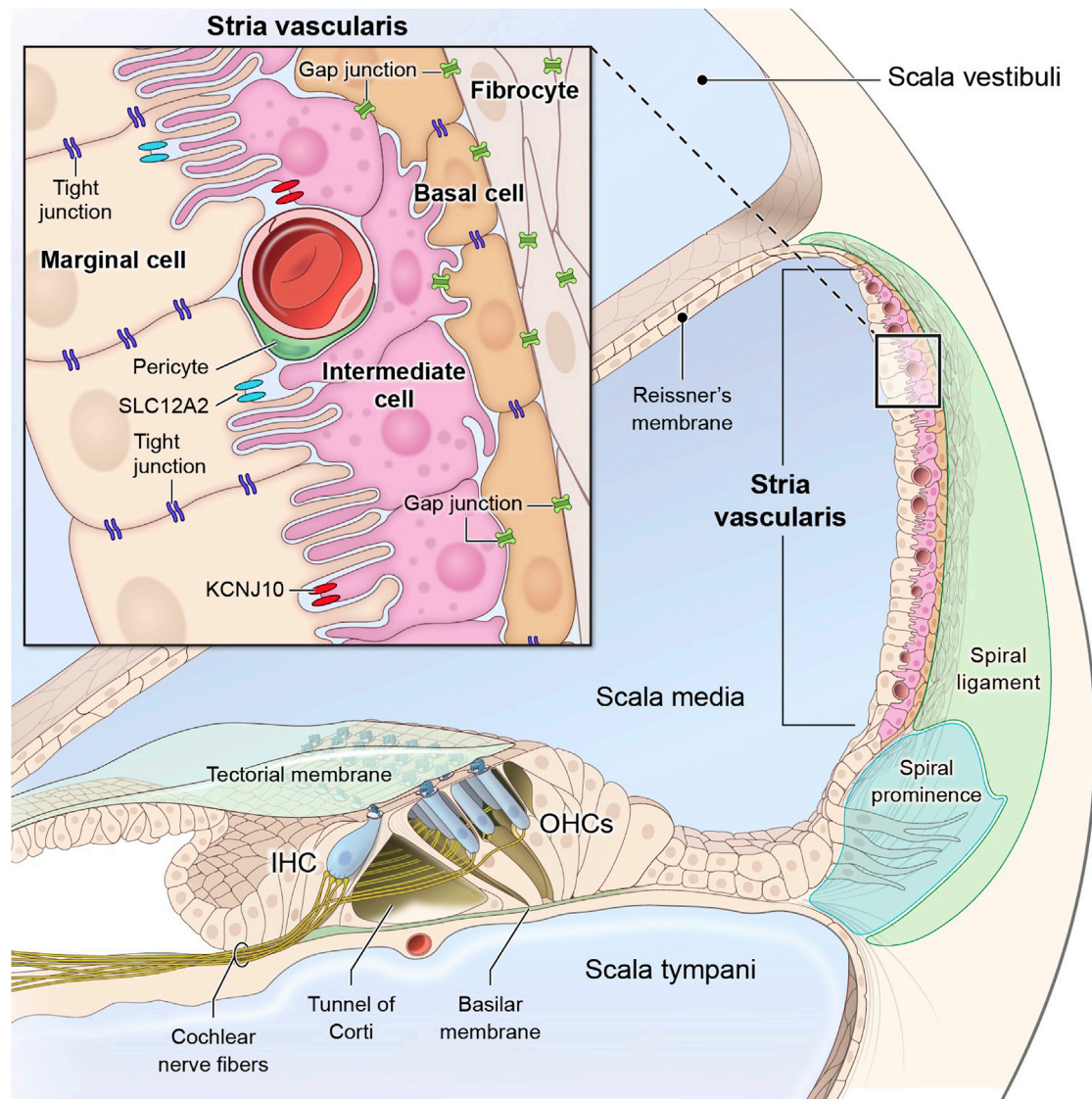
Figure 1. Cross-sectional anatomy of the scala media

The scala media contains the organ of Corti and the cochlear lateral wall. The endolymph, which bathes the hair bundles of the mechanosensory hair cells, has a high concentration of potassium ions. The cochlear lateral wall consists of the stria vascularis, spiral ligament, and spiral prominence. The stria vascularis contains three cell layers: the marginal, intermediate, and basal cell layers (inset). This figure was adapted from Faridi et al.[31] IHC, inner hair cell; OHC, outer hair cell.

by numerous mitochondria and by microvilli covering their apical-luminal surface. Mitochondria-rich cells express numerous proteins required to maintain ionic homeostasis, including SLC26A4 and ATP6V1B1.[33] *FOXI1* codes for the transcription factor FOXI1 and is considered a specific marker for mitochondria-rich cells in the endolymphatic sac. Recessive loss-of-function mutations of *FOXI1*, *SLC26A4,* and *ATP6V1B1* can all cause hereditary hearing loss. Given the important roles that the cochlear lateral wall and the endolymphatic sac play in hereditary hearing loss, it is important to develop effective gene therapies targeting cells in these regions. This requires the identification of efficient viral vectors that can transduce the large

number of cell types in the cochlear lateral wall and the endolymphatic sac.

There are several published studies that used various AAV serotypes to transduce the cochlear lateral wall and/or the endolymphatic sac. Chang et al. used AAV2/1 to deliver *Kcnq1* cDNA to the cochlear lateral wall of the *Kcnq1*$^{-/-}$ mice to rescue their hearing.[6] Wu et al. also used AAV1 to delivery *Kcne1* cDNA to the *Kcne1*$^{-/-}$ mice to rescue their auditory and vestibular functions.[17] Yu et al. used AAV2/1 to deliver *Gjb2* cDNA to a conditional *Gjb2* knockout mouse model to restore its gap junction network *in vivo*.[16] Similarly,
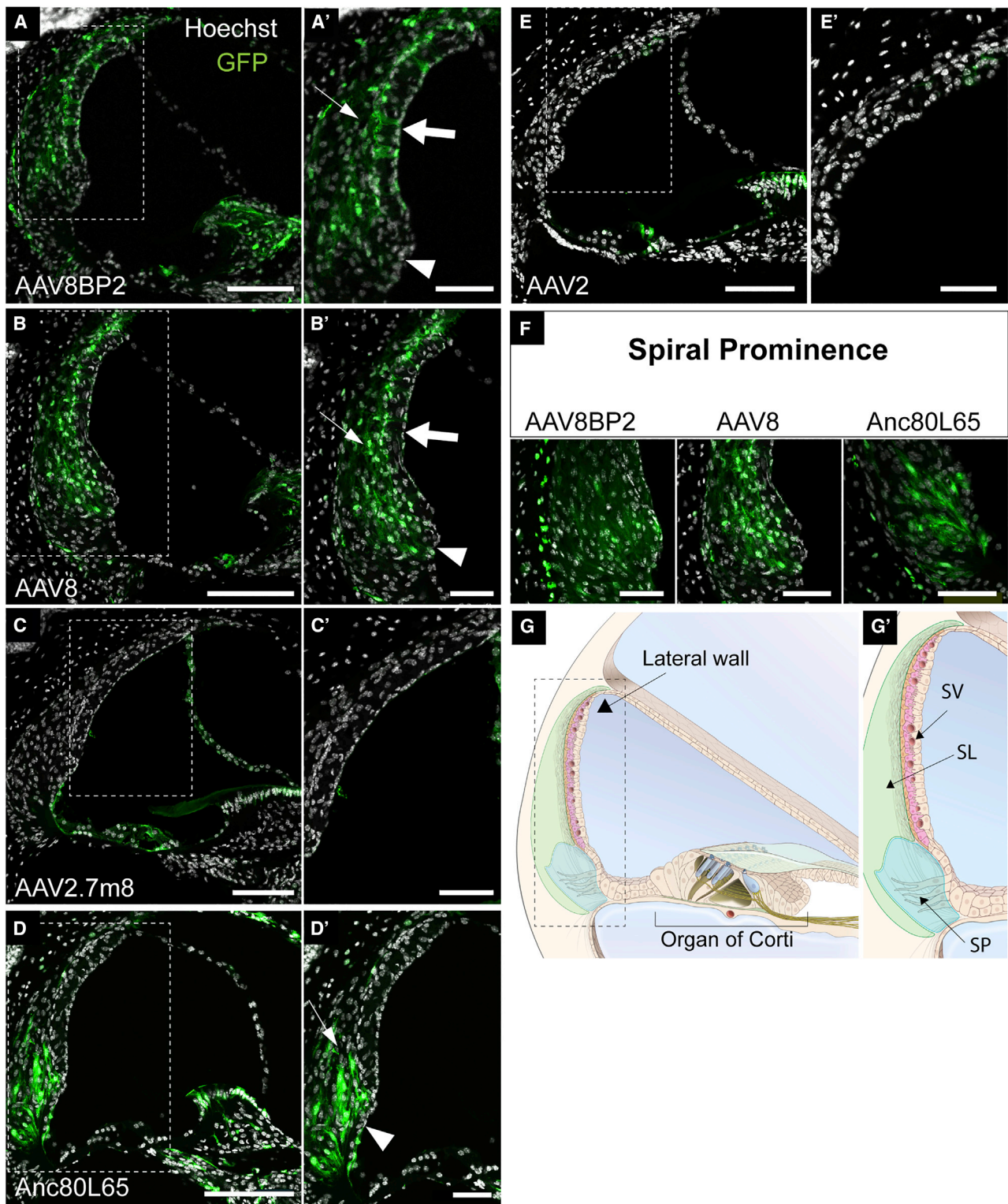
Figure 2. Cochlear lateral wall transduction patterns of different AAV serotypes

Representative confocal images of cross sections of the scala media in cochlear middle turn are shown (A–F). Enlarged images of the region of lateral wall are shown on the right of each panel (A'–E'). Enlarged images of the spiral prominence are presented in (F). AAV8BP2-GFP (A and A') and AAV8-GFP (B and B') transduced cells in the stria

(legend continued on next page)

Crispino et al. used bovine AAV to deliver *Gjb2* and *Gjb6* cDNAs to restore connexin 26 (Cx26) and connexin 30 (Cx30) expression in Cx26 and Cx30 conditional knockout mouse cochlear cultures *in vitro*, respectively.[35] Kim et al. used AAV2/1 to deliver *Slc26a4* cDNA to the otocyst of E12.5 *Slc26a4* mutant mice to improve their hearing.[36] SLC26A4 expression was detected in the endolymphatic sac.[36] While the results from these studies are promising, none of these studies specifically examined the transduction pattern and efficiency of a collection of different AAV serotypes for targeting the cochlear lateral wall and the endolymphatic sac.

In a previous study, we examined the transduction pattern and efficiency of two conventional AAVs (AAV2 and AAV8) and three synthetic AAVs (AAV2.7m8, AAV8BP2, Anc80L65) in the neonatal mouse sensory epithelium.[37] In this study, we examine the transduction pattern and efficiency of the same group of AAVs in the neonatal cochlear lateral wall. We find that AAV8BP2, AAV8, and Anc80L65 are capable of transducing various cell types in the cochlear lateral wall. In particular, AAV8BP2 and AAV8 can efficiently transduce the marginal cells and intermediate cells in the stria vascularis. We also show that AAV8BP2 and AAV8 are capable of targeting the mitochondria-rich cells and ribosome-rich cells of the endolymphatic sac when delivered through the posterior semicircular canal. In addition, we show that the diverse cell populations in the organ of Corti and the cochlear lateral wall can be successfully transduced by using AAV2.7m8 and AAV8BP2 simultaneously. Taken together, our data suggest that AAV8BP2 and AAV8 are highly useful viral vectors for inner ear gene therapy studies that target the cochlear lateral wall and the endolymphatic sac.

RESULTS

AAV8BP2, AAV8, and Anc80L65 transduce various cell types in the cochlear lateral wall

The cochlear lateral wall plays an important role in the ionic homeostasis of the cochlea.[38,39] Since many types of hereditary hearing loss are caused by mutations in genes expressed by cells in the cochlear lateral wall, we are interested in finding AAV serotypes that can efficiently target the various cell types in the cochlear lateral wall. We injected each of two conventional AAV-GFPs (AAV2 at 5.69×10^9 GC and AAV8 at 1.66×10^{10} GC) and each of three synthetic AAV-GFPs (AAV2.7m8 at 9.75×10^9 GC, AAV8BP2 at 1.10×10^{10} GC, Anc80L65 at 1.89×10^{10} GC) into neonatal (P0-P5) CBA/J mice using the posterior semicircular canal (PSC) approach.[37,40] The transduction patterns of the cochlear lateral wall were examined using cross-sectional images of the scala media at ~P30 (Figure 2). We found that AAV8BP2 transduced the stria vascularis, spiral prominence, spiral limbus, and spiral ligament in the cochlear lateral wall, as well as the cochlear hair cells. Examination of the stria vascularis at higher magnification showed GFP expression

in all three cellular layers. Examination of the spiral prominence showed transduction of the root cells. AAV8 also transduced the cochlear hair cells, spiral prominence, spiral limbus, stria vascularis, and spiral ligament. Consistent with our previous data, AAV2.7m8 was capable of transducing the cochlear hair cells and supporting cells in the sensory epithelium[37]; however, AAV2.7m8 had very limited ability to transduce the cochlear lateral wall. Anc80L65 was able to transduce the cochlear hair cells, spiral prominence, spiral limbus, and spiral ligament; however, the transduction of stria vascularis was limited. AAV2 was able to transduce the cochlear hair cells, but transduction of the cochlear lateral wall was very limited. In summary, our data suggest that AAV8BP2 and AAV8 are capable of transducing the stria vascularis, and AAV8BP2, AAV8, and Anc80L65 are capable of transducing the spiral prominence and spiral ligament in the cochlear lateral wall.

AAV8BP2 and AAV8 are capable of transducing the marginal cells in the stria vascularis

The stria vascularis is located in the lateral side of scala media and plays a critical role in K^+ recycling and in the generation and maintenance of endocochlear potential.[38,39,41] The marginal cells take up K^+ from the intrastrial space via the co-transporter SLC12A2 and ATP1A1/ATP1B2 and secrete K^+ into the endolymph via the transporter KCNQ1/KCNE1 in the apical plasma membrane.[38] In order to quantify the transduction efficiency of marginal cells by AAVs, whole-mount confocal microscopy images were acquired using anti-SLC12A2 antibody as a marker for marginal cells at ~P30. We found that both AAV8BP2 and AAV8 were capable of transducing the marginal cells, whereas AAV2.7m8, Anc80L65, and AAV2 transduced marginal cells at very low levels (Figure 3A). The mean ± SEM of marginal cell transduction efficiencies were 40.9% ± 8.49%, 11.17% ± 6.73%, 0.00% ± 0.00%, 0.46% ± 0.46%, and 1.02% ± 1.02% for AAV8BP2 (n = 9), AAV8 (n = 9), AAV2.7m8 (n = 4), Anc80L65 (n = 6), and AAV2 (n = 4), respectively (Figure 3B). The transduction efficiency for marginal cells was significantly higher for AAV8BP2 than AAV8, AAV2.7m8, Anc80L65, and AAV2 (p = 0.006, 0.003, 0.0007, and 0.003, respectively, one-way ANOVA with Bonferroni comparisons). We also examined the marginal cell transduction efficiency of AAV8BP2 and AAV8 at the middle and basal turns of the cochlea (Figure S1). We were unable to successfully obtain the lateral wall specimens from the cochlear apex because the cochlear perfusion process with paraformaldehyde was done through the apex and frequently damaged the lateral wall region in the cochlear apex. The marginal cell transduction rate of AAV8BP2 was 31.58% ± 13.69% at the middle turn (n = 4), and 48.35% ± 10.77% at the basal turn of the cochlea (n = 5). The difference in transduction rates for AAV8BP2 between the middle and basal turns was not statistically significant (p = 0.36, t test). The marginal cell transduction rate of AAV8 was 19.01% ± 11.29% at the middle turn

vascularis (thick white arrows). AAV8BP2-GFP (A and A'), AAV8-GFP (B and B'), and Anc80L65-GFP (D and D') transduced cells in the spiral ligament (thin white arrows), and spiral prominence (white arrowhead). Minimal cochlear lateral wall transduction was seen with AAV2.7m8-GFP (C and C') and AAV2-GFP (E and E'). Schematics of the scala media (G) and cochlear lateral wall (G') are shown for illustration. All images were taken at ~P30. Scale bars for (A–E) represent 100 μm. Scale bars for (A' to E') represent 50 μm. Scale bars for (F) represent 50 μm. SL, spiral ligament; SP, spiral prominence; SV, stria vascularis.
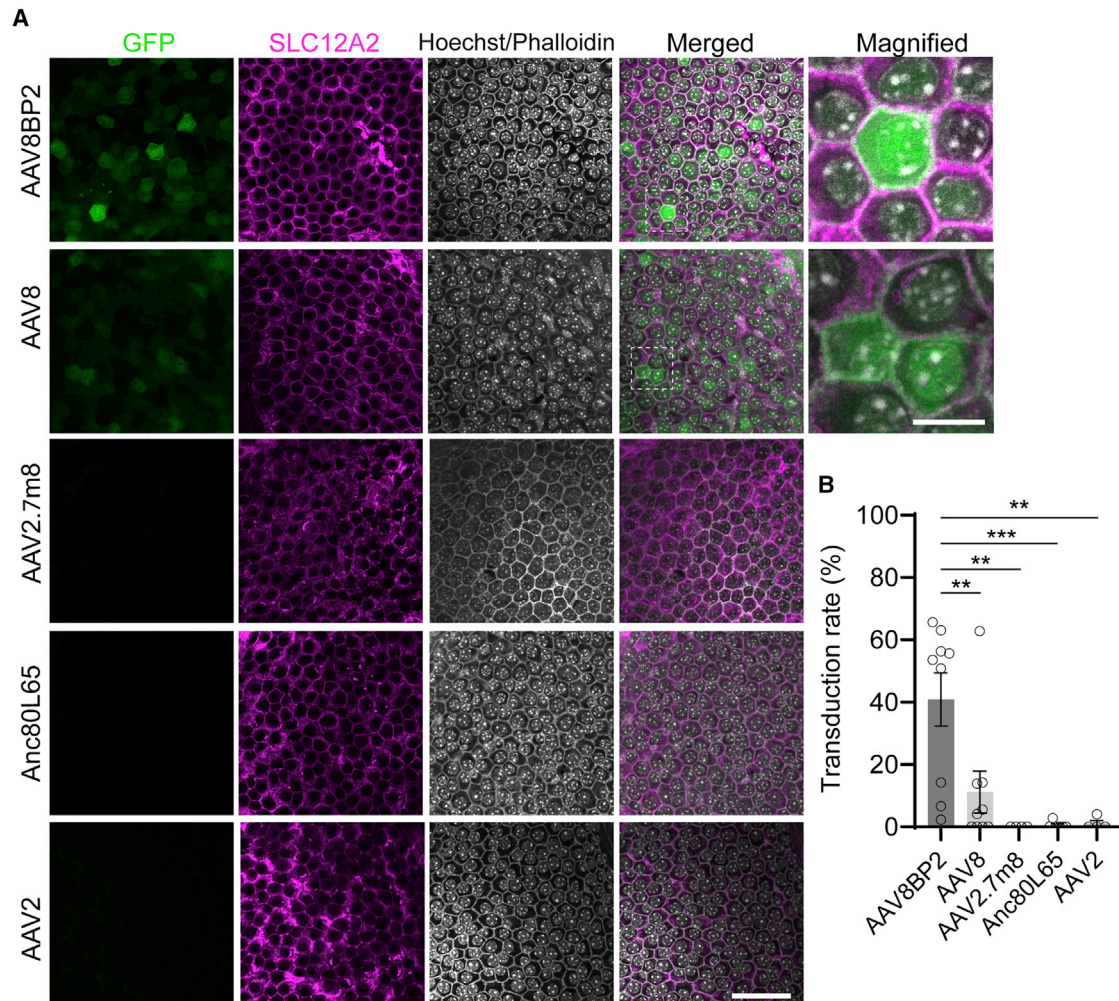
Figure 3. AAV8BP2-GFP and AAV8-GFP transduced the marginal cells in the stria vascularis

(A) Confocal images of the cochlear lateral wall at the level of the marginal cell layer are shown (single optical section). Anti-SLC12A2 antibody was used as a marginal cell marker. AAV8BP2-GFP (n = 9) and AAV8-GFP (n = 9) transduced the marginal cells in the stria vascularis, but AAV2.7m8-GFP (n = 4), Anc80L65-GFP (n = 6), and AAV2-GFP (n = 4) showed minimal marginal cell transduction. All images were taken at ∼P30. Surgeries were performed in P0–5 animals and the average surgery age was P2.0. The scale bar represents 50 μm for the lower-magnification images, and 10 μm for the magnified images. White dashed squares indicate areas where magnified images are taken. (B) Quantification of the marginal cell transduction efficiency with various AAV serotypes. Both individual (open circles) and average results are presented. **$p < 0.01$, ***$p < 0.001$. Error bars represent SEM.

(n = 5), and 1.39% ± 1.39% at the basal turn of the cochlea (n = 4). The difference in transduction rates for AAV8 between the middle and basal turns was not statistically significant (p = 0.21, t test). Our results suggest that, among the group of AAVs that we tested, AAV8BP2 and AAV8 transduce marginal cells most efficiently.

AAV8BP2 and AAV8 are capable of transducing the intermediate cells of the stria vascularis

The intermediate cells are located between the marginal cells and basal cells in the stria vascularis (Figure 1, inset). The intermediate cells secrete K^{+} into the intrastrial space via KCNJ10 channels, which is then taken up by the marginal cells and secreted into the endolymph.[38] We quantified the intermediate cell transduction efficiency of AAVs using anti-KCNJ10 antibody as a marker for intermediate cells at ∼P30. We found that AAV8BP2 and AAV8 were capable of transducing the intermediate cells efficiently, whereas AAV2.7m8, Anc80L65, and AAV2 transduced intermediate cells at very low levels (Figure 4A). The mean ± SEM of intermediate cell transduction efficiency for AAV8BP2 (n = 9), AAV8 (n = 9), AAV2.7m8 (n = 4), Anc80L65 (n = 5), and AAV2 (n = 4), were 26.0% ± 6.85%, 9.32% ± 6.25%, 0.00% ± 0.00%, 1.51% ± 1.01%, and 0.00% ± 0.00%, respectively (Figure 4B). The mean intermediate cell transduction efficiency for AAV8BP2 was not significantly different from that of AAV8 (p = 0.12), but it was significantly higher than those of AAV2.7m8, Anc80L65, and AAV2 (p = 0.04, p = 0.04, p = 0.04, respectively, one-way ANOVA with Bonferroni comparisons). We
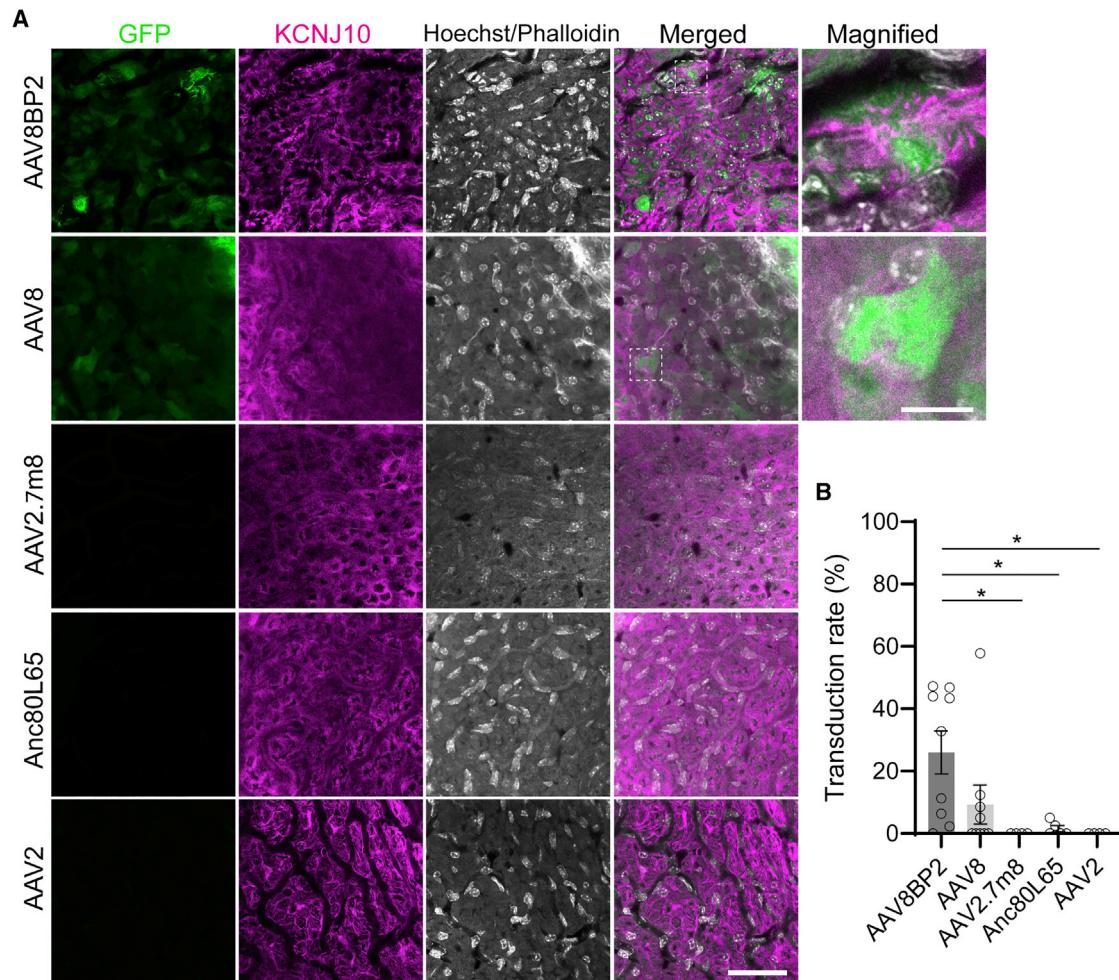
Figure 4. AAV8BP2-GFP and AAV8-GFP transduced the intermediate cells in the stria vascularis

(A) Confocal images of the cochlear lateral wall at the level of the intermediate cell layer are shown (single optical section). Anti-KCNJ10 antibody was used as an intermediate cell marker. AAV8BP2-GFP (n = 9) and AAV8-GFP (n = 9) transduced the intermediate cells in the stria vascularis, but AAV2.7m8-GFP (n = 4), Anc80L65-GFP (n = 5), and AAV2-GFP (n = 4) showed minimal intermediate cell transduction. All images were taken at ~P30. Surgeries were performed in P0–5 animals and the average surgery age was P1.9. The scale bar represents 50 μm for the lower-magnification images, and 10 μm for the magnified images. White dashed squares indicate areas where magnified images are taken. (B) Quantification of the intermediate cell transduction efficiency with various AAV serotypes. Both individual (open circles) and average results are presented. *p < 0.05. Error bars represent SEM.

also examined the intermediate cell transduction efficiency of AAV8BP2 and AAV8 at the middle and basal turns of the cochlea (Figure S2). The intermediate cell transduction rate of AAV8BP2 was 23.11% ± 12.72% at the middle turn (n = 4), and 28.32% ± 8.35% at the basal turn of the cochlea (n = 5). The difference in transduction rates for AAV8BP2 between the middle and basal turns was not statistically significant (p = 0.73, t test). The intermediate cell transduction rate of AAV8 was 15.76% ± 10.79% at the middle turn (n = 5), and 1.27% ± 1.27% at the basal turn of the cochlea (n = 4). The difference in transduction rates for AAV8 between the middle and basal turns was not statistically significant (p = 0.28, t test). Our results demonstrate that AAV8BP2 and AAV8 are capable of transducing the intermediate cells in the stria vascularis.

AAV8BP2 and AAV8 are capable of transducing the cells of the endolymphatic sac

Since AAV8BP2 and AAV8 could transduce cells in the cochlear lateral wall efficiently, we sought to determine if these vectors could also transduce cells in the endolymphatic sac. For this experiment, the Tg(ATP6V1B1-Cre):Ai14/+ mice were used to facilitate visualization of the endolymphatic sac, since cells of the endolymphatic sac show a mosaic expression of the tdTomato reporter.[32] AAV8BP2-GFP (n = 5) and AAV8-GFP (n = 4) were injected into the inner ear using the PSC approach at P0, and the endolymphatic sac was dissected for analysis at ~P30. We used anti-FOXI1 antibody as a marker for the mitochondria-rich cells in the endolymphatic sac. We found that both AAV8BP2 and AAV8
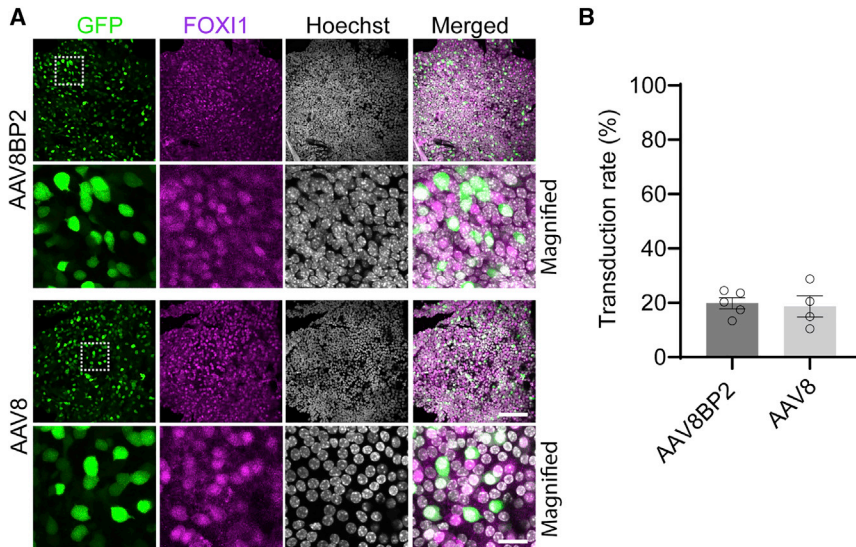
Figure 5. AAV8BP2-GFP and AAV8-GFP transduced cells of the endolymphatic sac

(A) Confocal images of the endolymphatic sac are shown. Anti-FOXI1 antibody was used as a marker for the mitochondria-rich cells in the endolymphatic sac. AAV8BP2-GFP (n = 5) and AAV8-GFP (n = 4) are both capable of transducing FOXI1-positive and FOXI1-negative cells in the endolymphatic sac. Surgeries were performed in P0 animals. The scale bar represents 50 μm for the lower-magnification images, and 20 μm for the magnified images. White dashed squares indicate areas where magnified images are taken. All images were taken at ∼P30. (B) Quantification of the endolymphatic sac transduction efficiency with AAV8BP2-GFP and AAV8-GFP. Both individual (open circles) and average results are presented. Error bars represent SEM.

were capable of transducing the cells of the endolymphatic sac with and without FOXI1 immunoreactivity (Figure 5). The mean endolymphatic sac transduction rates ± SEM were 19.86% ± 2.06% and 18.68% ± 3.93% for AAV8BP2 and AAV8, respectively (p = 0.79, t test). These results suggest that AAV8BP2 and AAV8 are both capable of transducing mitochondria-rich cells and ribosome-rich cells of the endolymphatic sac when injected via the PSC approach in the neonatal mouse inner ear.

Injection of AAV8BP2 at a lower concentration resulted in transduction of cochlear lateral wall without ABR threshold shift

In a previous study, we showed that neonatal CBA/J mice that underwent AAV8BP2-GFP injection (1.10×10^{10} GC) developed a 10–25 dB auditory brainstem response (ABR) threshold elevation and a small but statistically significant increase in circling behavior compared with non-injected control mice.[37] We also found that this effect on auditory and vestibular functions could be eliminated by decreasing the viral titer to 5.50×10^9 GC.[37] When we injected 5.50×10^9 GC of AAV8BP2-GFP into neonatal CBA/J ears using the PSC approach, we found that it was able to transduce the marginal cells and intermediate cells in the stria vascularis (Figure 6A). The mean transduction rates ± SEM for the marginal cells and the intermediate cells were 10.32% ± 9.47% (n = 4) and 5.61% ± 4.83% (n = 4), respectively. The transduction rates were lower compared with the mice that received 1.10×10^{10} GC of AAV8BP2-GFP. Consistent with our previous results, mice that received 5.50×10^9 GC of AAV8BP2-GFP did not have any significant ABR threshold elevation (Figure 6B) or increased circling behavior (Figure 6C) compared with non-injected control mice. These results suggest that at lower viral concentration, AAV8BP2 is still capable of transducing the marginal cells and intermediate cells in the stria vascularis, albeit at lower efficiencies.

Combined AAV2.7m8 and AAV8BP2 gene delivery is capable of transducing a diverse cell population in the cochlea

Since some of the most common causes of hereditary hearing loss are caused by mutations in genes that are expressed in diverse cell populations in the cochlea (e.g., *GJB2*), we decided to test if we could use the combination of AAV2.7m8 and AAV8BP2 to target the organ of Corti and the cochlear lateral wall simultaneously. We combined 0.5 μL of AAV2.7m8-GFP (4.88×10^9 GC) and 0.5 μL of AAV8BP2-GFP (5.50×10^9 GC) and injected this viral mixture into the inner ear of neonatal (P0-P5) CBA/J mice via the PSC approach. Examination of the cochlea at ∼P30 showed transduction of a diverse cellular population, including the inner and outer hair cells, supporting cells, cells in the stria vascularis, spiral ligament, spiral prominence, and spiral limbus (Figure 7A). The average marginal cell transduction rate was 20.99% ± 5.68% (n = 9), and the average intermediate cell transduction rate was 19.57% ± 7.68% (n = 9).

We tested the auditory and vestibular functions in mice that underwent the combined AAV2.7m8-GFP and AAV8BP2-GFP gene delivery. The auditory function was assessed using ABR at ∼P30. ABRs showed no significant difference in the injected mice compared with non-injected controls, indicating the preservation of the auditory system (two-way ANOVA with Bonferroni's multiple comparison, Figure 7B). The vestibular function was assessed by examining the circling behavior in these animals at ∼P30. Mice that underwent combined AAV2.7m8-GFP and AAV8BP2-GFP gene delivery showed no significant increase in circling behavior, indicating the preservation of the vestibular system (unpaired t test, Figure 7C). Our results demonstrate that the combination of AAV2.7m8 and AAV8BP2 can target a diverse cellular population in both the organ of Corti and the cochlear lateral wall simultaneously, while preserving the auditory and vestibular functions in these animals.
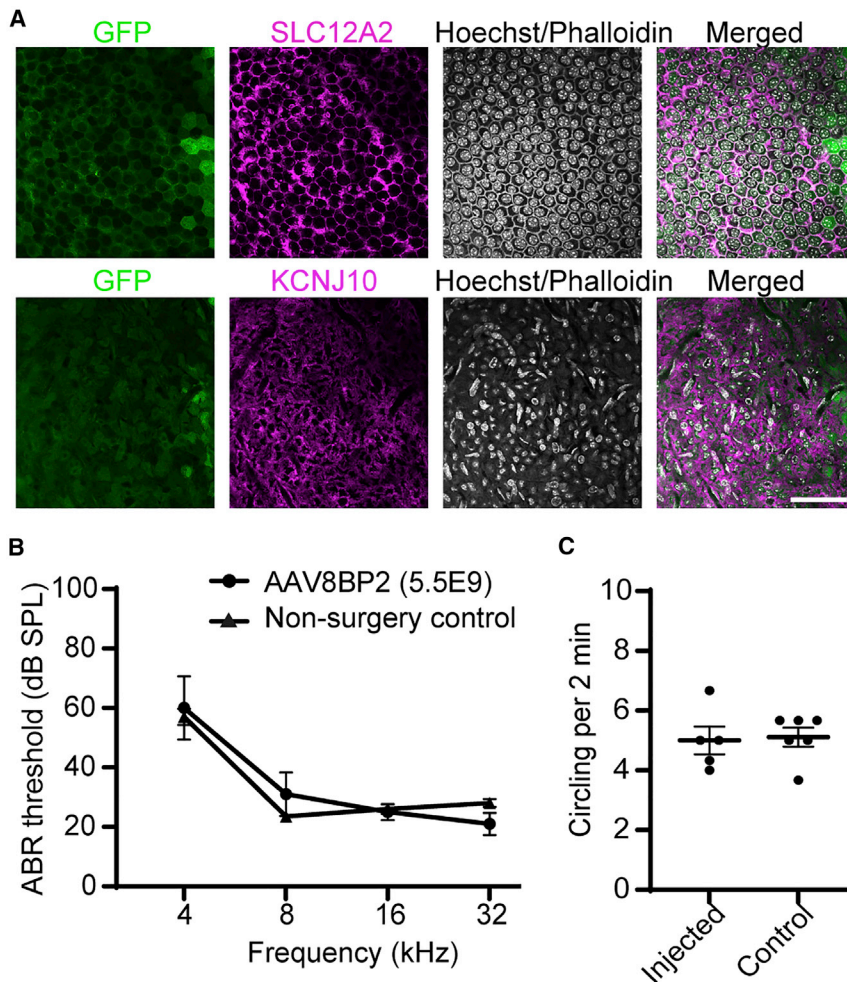
Figure 6. Lowered AAV8BP2-GFP titer transduced the cochlear lateral wall without causing ABR threshold elevation

(A) Confocal images of the marginal cell layer (top row) and the intermediate cell layer (bottom row) of the stria vascularis in mice are shown. Transduction of the marginal cells and intermediate cells are seen in these animals, despite at lower viral concentration (5.50×10^9 GC). Scale bar represents 50 μm. (B) ABR thresholds of mice that were injected with 5.50×10^9 GC of AAV8BP2-GFP are shown (labeled "AAV8BP2 (5.5E9)," n = 5). No significant ABR threshold elevation was seen in these animals compared with non-injected control mice (labeled "Non-surgery control," n = 10). (C) Circling behavior of mice that were injected with 5.50×10^9 GC of AAV8BP2-GFP (labeled "Injected," n = 5) is shown. No significant elevation in circling behavior was observed in these animals compared with non-injected control mice (labeled "Control," n = 6). Surgeries were performed in P0–5 animals and the average surgery age was P4.4. Error bars represent SEM.

ear gene delivery as a treatment for diseases affecting these cell types. Our study showed that AAV8BP2 and AAV8 are capable of transducing the marginal cells and intermediate cells efficiently. This suggests that AAV8BP2 and AAV8 may be useful for AAV-mediated inner ear gene therapy studies targeting mutations affecting genes expressed in the stria vascularis, such as *KCNQ1/KCNE1* and *KCNJ10*.

Our study also showed that in addition to the stria vascularis, AV8BP2 and AAV8 are capable of transducing the spiral prominence and endolymphatic sac simultaneously, when injected through the PSC. These results suggest that AAV8BP2 and AAV8 may be good viral vectors for inner ear gene therapy studies targeting genes such as *SLC26A4*. *SLC26A4* encodes pendrin, which is an anion exchanger transporting Cl^- and HCO3− in the inner ear. Mutations in *SLC26A4* cause the non-syndromic autosomal recessive hereditary hearing loss DFNB4, as well as Pendred syndrome, which is one of the most common types of syndromic hereditary hearing loss.[47,48] In a previous study by Kim et al., AAV2/1 was used to deliver *Slc26a4* cDNA to the otocyst of E12.5 *Slc26a4* mutant mice to improve their hearing.[36] However, SLC26A4 expression was only detected in the endolymphatic sac, but not in the cochlea and the vestibular organs. The auditory function remained unstable and the vestibular function was not restored in these mice.[36] Our results suggest that both AAV8BP2 and AAV8 are potentially useful viral vectors for inner ear gene therapy studies in mouse models of Pendred syndrome.

Previously, we showed that AAV8BP2-GFP at high viral titer (1.10×10^{10} GC) can lead to a small but significant ABR threshold

DISCUSSION

The cochlear lateral wall consists of the stria vascularis, spiral prominence, and spiral ligament, and it plays an important role in potassium recycling and the generation and maintenance of endocochlear potential.[38,39] Tight control of endocochlear potential is critical for the proper functioning of the cochlea.[42] Mutations in genes expressed by cells in the cochlear lateral wall, such as *KCNQ1/KCNE1*, *KCNJ10*, *SLC26A4*, and *CLDN14*, account for a large portion of hereditary hearing loss.[26,43] In addition, the cochlear lateral wall may play an important role in age-related hearing loss, which is by far the most common type of hearing loss.[44] It has been shown that the stria vascularis undergoes degeneration with aging.[45] It has also been shown that the expression of KCNJ10, an inwardly rectifying potassium channel found in the intermediate cells in the stria vascularis, undergoes significant alteration with aging, suggesting that the potassium recycling process mediated by the stria vascularis may be impaired with aging.[46] Given the importance of the cochlear lateral wall at maintaining proper cochlear function, and its involvement with multiple types of hearing loss, it is critical to identify viral vectors that can effectively target various cell types in the cochlear lateral wall for potential inner
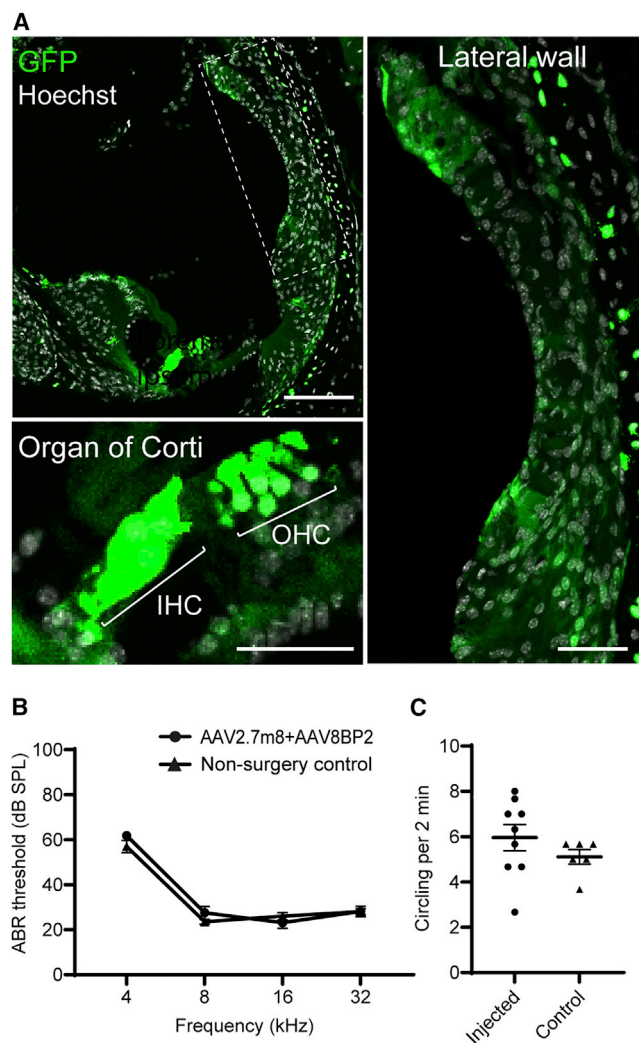
Figure 7. Combined AAV2.7m8-GFP and AAV8BP2-GFP injection transduced diverse cell types throughout the cochlea

(A) Confocal images of a cross section of the scala media of a mouse that underwent combined AAV2.7m8-GFP (4.88×10^9 GC) and AAV8BP2-GFP (5.50×10^9 GC) inner ear injection via the PSC approach. Enlarged images of the regions of the cochlear lateral wall (right) and the organ of Corti (below) are also shown. GFP expression is seen in the inner/outer hair cells (IHC/OHC), supporting cells, stria vascularis, spiral prominence, and spiral ligament. The scale bar for the lower-magnification image (upper left) represents 100 μm, and the scale bars for the higher-magnification images (labeled "Organ of Corti" and "Lateral wall") represent 50 μm. (B) ABR thresholds of mice injected with both AAV2.7m8-GFP and AAV8BP2-GFP (labeled "AAV2.7m8+AAV8BP2," n = 8) were compared with non-surgery animals (labeled "Non-surgery control," n = 10). There are no statistically significant differences in ABR thresholds between the two groups of animals at all four frequencies tested (4 kHz p = 0.39, 8 kHz p = 0.69, 16 kHz p > 0.99, 32 kHz p > 0.99). (C) Circling behavior in mice that were injected with both AAV2.7m8-GFP and AAV8BP2-GFP (labeled "Injected," n = 9) was compared with non-surgery mice (labeled "Control," n = 6). No significant increase in circling was seen in the injected animals compared with non-injected control mice, p = 0.29. Surgeries were performed in P0–5 animals and the average surgery age was P3.7. Error bars represent SEM.

elevation and increased circling.[37] In this study, we showed that AAV8BP2-GFP at lower titer (5.50×10^9 GC) can transduce the marginal cells and intermediate cells in the stria vascularis without any significant ABR threshold elevation or increase in circling behavior. However, the transduction rates were lower in both cell types compared with mice that received higher titer of the viral vector (1.10×10^{10} GC). It is important to point out that AAV-mediated GFP overexpression has been shown to cause toxicity.[49] Therefore, it is possible that AAV8BP2 can be an effective viral vector for gene delivery if the transgene overexpression does not cause toxicity in the inner ear. In addition, the transgene expression may also be modulated using various promoters, thereby lessening the potential toxicity caused by AAV8BP2-mediated inner ear gene delivery.

Over the past few years, several studies have shown that inner ear gene therapy can be successfully applied to various mouse models of hearing loss and dizziness to improve the auditory and vestibular functions in these animals.[18,50,51] Most of these studies focused on genes that are only expressed in a single cell type in the cochlea (e.g., *VGlut3* and inner hair cells). However, some of the most common forms of hereditary hearing loss are caused by mutations in genes that are expressed by a large number of cell types in the cochlea, such as *GJB2*. Therefore, we examined if we could use the combination of AAV2.7m8 and AAV8BP2 to transduce the diverse cellular population in the organ of Corti and the cochlear lateral wall simultaneously. We leveraged AAV2.7m8's ability to target the cochlear inner and outer hair cells and supporting cells, and AAV8BP2's ability to target the different cell types in the cochlear lateral wall, and showed that combined AAV2.7m8 and AAV8BP2 gene delivery could transduce a wide variety of cell types in the organ of Corti and the cochlear lateral wall (Figure 7A). Interestingly, we found that the marginal cell and intermediate cell transduction rates for combined AAV2.7m8-GFP and AAV8BP2-GFP gene delivery were higher (20.99% ± 5.68%, and 19.57% ± 7.68%, respectively) than AAV8BP2-GFP alone (10.32% ± 9.47%, and 5.61% ± 4.83%, respectively), even though the viral genome copies delivered in both cases were the same (5.50×10^9 GC). While the reason for this finding is unclear, one possible explanation is that when AAV8BP2 is delivered alone, it transduces the cochlear hair cells and the cochlear lateral wall; however, when AAV8BP2 and AAV2.7m8 are delivered simultaneously into the inner ear, AAV2.7m8 preferentially transduces the cochlear hair cells, thereby allowing more AAV8BP2 viral particles to transduce the cells in the cochlear lateral wall. Our results show that by understanding the tropisms of various AAV serotypes, one could apply this knowledge to use different combinations of AAVs to target different cell populations in the mammalian inner ear to achieve cell-specific transgene expression mimicking the endogenous expression of the gene targeted. This strategy can complement other strategies for cell-specific targeting, such as the use of cell-type specific promoters, which may enhance the efficacy and safety of inner ear gene therapy.

To our knowledge, our study is the first dedicated study to examine multiple AAV serotypes for targeting the mammalian cochlear lateral

wall. We also show that AAV8BP2 and AAV8 are capable of transducing the cells in the endolymphatic sac when injected through the PSC. In addition, the use of AAV2.7m8 and AAV8BP2 to target a large number of cell types in the mammalian cochlea simultaneously is also novel. It is our hope that these results will help to expand the application of inner ear gene therapy to the diverse cell populations in the mammalian inner ear.

MATERIALS AND METHODS

AAV vector construction
The AAV2.7m8-CAG-eGFP (9.75×10^{12} GC/mL), AAV8BP2-CAG-eGFP (1.10×10^{13} GC/mL), AAV2-CAG-eGFP (5.69×10^{12} GC/mL), AAV2/8-CAG-eGFP (1.66×10^{13} GC/mL), and Anc80L65-CAG-eGFP (1.89×10^{13} GC/mL) were produced by the Research Vector Core at the Center for Advanced Retinal and Ocular Therapeutics (University of Pennsylvania). The production method for these viruses has been previously described.[52] All viruses were produced using the same transgene construct, consisting of the CAG promoter derived from InvivoGen pDRIVE CAG plasmid (InvivoGen, San Diego, CA), the cDNA encoding enhanced GFP (eGFP) protein, and the bovine growth hormone (bGH) polyadenylation signal. The viral particles delivered to each animal is calculated by multiplying the viral concentration of each AAV serotype by the injection volume delivered. All viral vectors used in this study underwent endotoxin testing. The endotoxin levels were 0.20 EU/mL for AAV2.7m8, 0.23 EU/mL for AAV8BP2, 0.14 EU/mL for AAV2, 0.26 EU/mL for AAV2/8, and 0.22 EU/mL for Anc80L65.

Animal surgery
Animal surgery was approved by the joint Animal Care and Use Committee of the National Institute of Neurological Diseases and Stroke and the National Institute on Deafness and Other Communication Disorders (NIDCD ASP1378). All animal procedures were done in compliance with the ethical guidelines and regulations set forth by the Animal Care and Use Committee at NIDCD. CBA/J, B6; CBA-Tg(ATP6V1B1-Cre)[1Rnel/Mm], and B6.Cg-*Gt(ROSA)26Sor*[tm14(CAG-tdTomato)Hze]/J (Ai14) (Jackson Laboratory, Bar Harbor, ME) mice were used in this study. For neonatal mice (P0–P5), hypothermia was used to induce and maintain anesthesia. Surgery was performed only in the left ear of each animal. For inner ear gene delivery via the PSC approach, a post-auricular incision was made, and tissue was dissected to expose the PSC. Care was taken to avoid the facial nerve during the dissection. A Nanoliter Microinjection System (Nanoliter2000, World Precision Instruments, Sarasota, FL) was used in conjunction with a glass micropipette to load AAV-eGFP into the glass micropipette. A total of 1 µL of AAV-eGFP was injected over approximately 40 s. Incision was closed with 5-0 Vicryl sutures and tissue glue.

Auditory brainstem response
ABR testing was used to evaluate hearing sensitivity at ∼P30. Animals were anesthetized with ketamine (100 mg/kg) and dexmedetomidine (0.375 mg/kg) via intraperitoneal injections and placed on a warming pad inside a sound booth (ETS-Lindgren Acoustic Systems, Cedar Park, TX). The animal's temperature was maintained using a closed feedback loop and monitored using a rectal probe (TC-1000; CWE Incorporated, Ardmore, PA). Sub-dermal needle electrodes were inserted at the vertex (+) and test-ear mastoid (−) with a ground electrode under the contralateral ear. Stimulus generation and ABR recordings were completed using Tucker-Davis Technologies hardware (RZ6 Multi I/O Processor, Tucker-Davis Technologies, Gainesville, FL) and software (BioSigRx, v.5.1). ABR thresholds were measured at 4, 8, 16, and 32 kHz using 3-ms, Blackman-gated tone pips presented at 29.9/s with alternating stimulus polarity. At each stimulus level, 512 to 1,024 responses were averaged. Thresholds were determined by visual inspection of the waveforms and were defined as the lowest stimulus level at which any wave could be reliably detected. A minimum of two waveforms were obtained at the threshold level to ensure repeatability of the response. Physiological results were analyzed for individual frequencies, and then averaged for each of these frequencies from 4 to 32 kHz.

Circling behavior
The circling behavior of mice that underwent inner ear gene delivery was quantified using optical tracking and the ANY-maze tracking software (version 4.96; Stoelting Co., Wood Dale, IL). A 38 cm × 58-cm box was attached to a video camera (Fujinon YV5X2.7R4B-2 1/3-inch 2.7–13.5mm F1.3 Day/Night Aspherical Vari-Focal Lens). The ANY-maze video tracking software was set to track the head of mice placed within the box. Each mouse was placed into the box and allowed to acclimate to the new environment for 2 min. Complete rotations were recorded and quantified for the next 2 min, followed by a 1-min "cool-down" period where rotations were not tracked. Each mouse was assessed three times, and the average was taken.

Immunohistochemistry and quantification
After completion of functional testing, mice were euthanized by CO_2 asphyxiation followed by decapitation. Temporal bones were harvested and fixed with 4% paraformaldehyde diluted in phosphate-buffered saline (PBS), followed by decalcification in 120 mM EDTA for 4 to 7 days. The cochlear tissues were micro-dissected into base, middle, and apical turns. The basal and middle turns of the cochlear lateral wall were dissected out separately (we were unable to successfully obtain the lateral wall specimens from the cochlear apex because the cochlear perfusion process with paraformaldehyde frequently damages this region of the lateral wall). Tissues were washed in PBS, and blocked/permeabilized with 2% BSA and goat serum with 0.5% Triton X-100 in PBS for 2 h. Incubation with primary antibody was performed overnight at 4°C. The dissection of the endolymphatic sac has been previously described.[32] After washing with PBS, endolymphatic sac was blocked/permeabilized with 5% normal donkey serum and 0.5% Triton X-100 in PBS. For the primary antibodies, SLC12A2 antibodies were used to label marginal cells (1:100, Cat# sc21545; Santa Cruz Biotech, Dallas, TX), and KCNJ10 antibodies for intermediate cells (1:100, Cat# APC-035; Alomone Labs, Jerusalem, Israel).[53] Antibodies directed against FOXI1 were used to label mitochondria-rich cells in the endolymphatic sac (1:200, Cat#

ab20454; Abcam, Cambridge, MA). Phalloidin (1:50, Phalloidin-Atto 390, Cat#50556; Sigma-Aldrich, St. Louis, MO), Alexa Fluor 546, donkey anti-goat immunoglobulin (Ig)G (Cat# A-11056; Invitrogen, Carlsbad, CA), Alexa Fluor 647, donkey anti-rabbit IgG (Cat# A-31573; Invitrogen), were applied for 2 h at room temperature for lateral wall tissues. Alexa Flour 647, donkey anti-goat IgG (Cat# A-21447; Invitrogen) were applied for 1 h at room temperature for the endolymphatic sac. Hoechst stain was used to label nuclei (1:300, Cat# 62,249; Life Technologies, Carlsbad, CA). Primary and secondary antibodies were diluted in PBS. For cross sections, cochleae were collected and fixed overnight with 4% paraformaldehyde diluted in PBS, followed by decalcification in EDTA for 4 to 5 days and embedded in SCEM freezing media (Cat# C-EM001; Section-Lab Co, Kanagawa, Japan); 12-μm sections were collected using Leica CM3050S cryostat. Images were obtained using z stack with Zeiss LSM880 confocal microscope (Zeiss Microimaging, Inc, Jena, Germany) at Plan-Neofluar ×10/0.30 and Plan-Neofluaromat ×40/1.3 Oil DIC M27 for cochlea and Plan-Neofluaromat ×40/1.3 Oil DIC M27 for lateral wall, and Plan-Neofluar ×10/0.30 and Plan-Neofluaromat ×20/0.8 for cross sections.

Marginal cells were identified as hexagon-shaped cells forming a single layer in the z-stack images and confirmed by their expression of SLC12A2 and counted. Marginal cell transduction rate was obtained by manually counting the number of GFP-positive cells co-labeled with SLC12A2, and dividing this number by the total marginal cell count. The average from two locations in each specimen was taken. Since the intermediate cells are polymorphous in shape, quantification of total intermediate cell count was performed by manually counting the number of cells whose nuclei were surrounded by KCNJ10 expression using z-stack images. Intermediate cell transduction rate was calculated by counting the number of GFP-positive cells that co-labeled with KCNJ10 and dividing this number by the total intermediate cell count. The average from two locations of each specimen was taken. It is important to note that marginal cells and intermediate cells project toward each other and SLC12A2 and KCNJ10 expressions partially overlapped. We only counted intermediate cells that expressed GFP and KCNJ10 starting where a minimal amount of SLC12A2 expression was seen and counted nuclei surrounded by KCNJ10 signals using z-stack images. Images of the whole endolymphatic sac were obtained as maximal intensity projections of z stacks at ×40 magnification. The endolymphatic sac has multiple folds, and this method ensures that the entire endolymphatic sac is visualized. For transduction rate quantification in the endolymphatic sac, GFP-positive cells were counted and compared with the total number of cellular nuclei identified using Hoechst stain throughout the z stack.

Statistics
GraphPad Prism version 9.2.0. was used for statistical analysis. Ordinary one-way ANOVA with multiple comparisons was used to assess the differences in transduction rate for marginal cells and intermediate cells among various virus serotypes. Two-way ANOVA with multiple comparisons was used to assess the differences in ABR thresholds. Two-tailed unpaired t test was used for the circling behavior and endolymphatic sac transduction. A p-value < 0.05 indicates statistical significance.

DATA AVAILABILITY STATEMENT
The data in this study are available upon request.

SUPPLEMENTAL INFORMATION
Supplemental information can be found online at https://doi.org/10.1016/j.omtm.2022.07.013.

AUTHOR CONTRIBUTIONS
W.C., J.B., D.M., I.R., and A.G. conceived and designed the study. K.I., Y.I., HJ.L., J.Z., and W.C. performed and analyzed the experiments. W.C. and I.R. supervised the work. M.G. and I.R. provided support for the study. Y.I., W.C., and K.I. wrote the manuscript with participation of all authors.

DECLARATION OF INTERESTS
J.B. is a co-author on a patent for AAV8BP2.

REFERENCES
1. Naso, M.F., Tomkowicz, B., Perry, W.L., 3rd, and Strohl, W.R. (2017). Adeno-associated virus (AAV) as a vector for gene therapy. BioDrugs *31*, 317–334. https://doi.org/10.1007/s40259-017-0234-5.

2. Akil, O., Seal, R.P., Burke, K., Wang, C., Alemi, A., During, M., Edwards, R.H., and Lustig, L.R. (2012). Restoration of hearing in the VGLUT3 knockout mouse using virally mediated gene therapy. Neuron *75*, 283–293. https://doi.org/10.1016/j.neuron.2012.05.019.

3. Akil, O., Dyka, F., Calvet, C., Emptoz, A., Lahlou, G., Nouaille, S., Boutet de Monvel, J., Hardelin, J.P., Hauswirth, W.W., Avan, P., et al. (2019). Dual AAV-mediated gene therapy restores hearing in a DFNB9 mouse model. Proc. Natl. Acad. Sci. USA *116*, 4496–4501. https://doi.org/10.1073/pnas.1817537116.

4. Al-Moyed, H., Cepeda, A.P., Jung, S., Moser, T., Kügler, S., and Reisinger, E. (2019). A dual-AAV approach restores fast exocytosis and partially rescues auditory function in deaf otoferlin knock-out mice. EMBO Mol. Med. *11*, e9396. https://doi.org/10.15252/emmm.201809396.

5. Askew, C., Rochat, C., Pan, B., Asai, Y., Ahmed, H., Child, E., Schneider, B.L., Aebischer, P., and Holt, J.R. (2015). Tmc gene therapy restores auditory function in deaf mice. Sci. Transl. Med. *7*, 295ra108. https://doi.org/10.1126/scitranslmed.aab1996.

6. Chang, Q., Wang, J., Li, Q., Kim, Y., Zhou, B., Wang, Y., Li, H., and Lin, X. (2015). Virally mediated Kcnq1 gene replacement therapy in the immature scala media

restores hearing in a mouse model of human Jervell and Lange-Nielsen deafness syndrome. EMBO Mol. Med. 7, 1077–1086. https://doi.org/10.15252/emmm.201404929.

7. Chien, W.W., Isgrig, K., Roy, S., Belyantseva, I.A., Drummond, M.C., May, L.A., Fitzgerald, T.S., Friedman, T.B., and Cunningham, L.L. (2016). Gene therapy restores hair cell stereocilia morphology in inner ears of deaf whirler mice. Mol. Ther. 24, 17–25. https://doi.org/10.1038/mt.2015.150.

8. Dulon, D., Papal, S., Patni, P., Cortese, M., Vincent, P.F., Tertrais, M., Emptoz, A., Tlili, A., Bouleau, Y., Michel, V., et al. (2018). Clarin-1 gene transfer rescues auditory synaptopathy in model of Usher syndrome. J. Clin. Invest. 128, 3382–3401. https://doi.org/10.1172/JCI94351.

9. Emptoz, A., Michel, V., Lelli, A., Akil, O., Boutet de Monvel, J., Lahlou, G., Meyer, A., Dupont, T., Nouaille, S., Ey, E., et al. (2017). Local gene therapy durably restores vestibular function in a mouse model of Usher syndrome type 1G. Proc. Natl. Acad. Sci. USA 114, 9695–9700. https://doi.org/10.1073/pnas.1708894114.

10. Geng, R., Omar, A., Gopal, S.R., Chen, D.H.C., Stepanyan, R., Basch, M.L., Dinculescu, A., Furness, D.N., Saperstein, D., Hauswirth, W., et al. (2017). Modeling and preventing progressive hearing loss in usher syndrome III. Sci. Rep. 7, 13480. https://doi.org/10.1038/s41598-017-13620-9.

11. György, B., Sage, C., Indzhykulian, A.A., Scheffer, D.I., Brisson, A.R., Tan, S., Wu, X., Volak, A., Mu, D., Tamvakologos, P.I., et al. (2017). Rescue of hearing by gene delivery to inner-ear hair cells using exosome-associated AAV. Mol. Ther. 25, 379–391. https://doi.org/10.1016/j.ymthe.2016.12.010.

12. Isgrig, K., Shteamer, J.W., Belyantseva, I.A., Drummond, M.C., Fitzgerald, T.S., Vijayakumar, S., Jones, S.M., Griffith, A.J., Friedman, T.B., Cunningham, L.L., and Chien, W.W. (2017). Gene therapy restores balance and auditory functions in a mouse model of usher syndrome. Mol. Ther. 25, 780–791. https://doi.org/10.1016/j.ymthe.2017.01.007.

13. Kim, M.A., Cho, H.J., Bae, S.H., Lee, B., Oh, S.K., Kwon, T.J., Ryoo, Z.Y., Kim, H.Y., Cho, J.H., Kim, U.K., and Lee, K.Y. (2016). Methionine sulfoxide reductase B3-targeted in utero gene therapy rescues hearing function in a mouse model of congenital sensorineural hearing loss. Antioxid. Redox Signal. 24, 590–602. https://doi.org/10.1089/ars.2015.6442.

14. Nist-Lund, C.A., Pan, B., Patterson, A., Asai, Y., Chen, T., Zhou, W., Zhu, H., Romero, S., Resnik, J., Polley, D.B., et al. (2019). Improved TMC1 gene therapy restores hearing and balance in mice with genetic inner ear disorders. Nat. Commun. 10, 236. https://doi.org/10.1038/s41467-018-08264-w.

15. Pan, B., Askew, C., Galvin, A., Heman-Ackah, S., Asai, Y., Indzhykulian, A.A., Jodelka, F.M., Hastings, M.L., Lentz, J.J., Vandenberghe, L.H., et al. (2017). Gene therapy restores auditory and vestibular function in a mouse model of Usher syndrome type 1c. Nat. Biotechnol. 35, 264–272. https://doi.org/10.1038/nbt.3801.

16. Yu, Q., Wang, Y., Chang, Q., Wang, J., Gong, S., Li, H., and Lin, X. (2014). Virally expressed connexin26 restores gap junction function in the cochlea of conditional Gjb2 knockout mice. Gene Ther. 21, 71–80. https://doi.org/10.1038/gt.2013.59.

17. Wu, X., Zhang, L., Li, Y., Zhang, W., Wang, J., Cai, C., and Lin, X. (2021). Gene therapy via canalostomy approach preserves auditory and vestibular functions in a mouse model of Jervell and Lange-Nielsen syndrome type 2. Nat. Commun. 12, 697. https://doi.org/10.1038/s41467-020-20808-7.

18. Askew, C., and Chien, W.W. (2020). Adeno-associated virus gene replacement for recessive inner ear dysfunction: progress and challenges. Hear. Res. 394, 107947. https://doi.org/10.1016/j.heares.2020.107947.

19. Patuzzi, R. (2011). Ion flow in stria vascularis and the production and regulation of cochlear endolymph and the endolymphatic potential. Hear. Res. 277, 4–19. https://doi.org/10.1016/j.heares.2011.01.010.

20. Hibino, H., Nin, F., Tsuzuki, C., and Kurachi, Y. (2010). How is the highly positive endocochlear potential formed? The specific architecture of the stria vascularis and the roles of the ion-transport apparatus. Pflugers Arch. 459, 521–533. https://doi.org/10.1007/s00424-009-0754-z.

21. Jagger, D.J., and Forge, A. (2013). The enigmatic root cell - emerging roles contributing to fluid homeostasis within the cochlear outer sulcus. Hear. Res. 303, 1–11. https://doi.org/10.1016/j.heares.2012.10.010.

22. Furness, D.N. (2019). Forgotten fibrocytes: a neglected, supporting cell type of the cochlea with the potential to be an alternative therapeutic target in hearing loss. Front. Cell. Neurosci. 13, 532. https://doi.org/10.3389/fncel.2019.00532.

23. Hibino, H., Higashi-Shingai, K., Fujita, A., Iwai, K., Ishii, M., and Kurachi, Y. (2004). Expression of an inwardly rectifying K+ channel, Kir5.1, in specific types of fibrocytes in the cochlear lateral wall suggests its functional importance in the establishment of endocochlear potential. Eur. J. Neurosci. 19, 76–84. https://doi.org/10.1111/j.1460-9568.2004.03092.x.

24. Jagger, D.J., Nevill, G., and Forge, A. (2010). The membrane properties of cochlear root cells are consistent with roles in potassium recirculation and spatial buffering. J. Assoc. Res. Otolaryngol. 11, 435–448. https://doi.org/10.1007/s10162-010-0218-3.

25. Morton, C.C., and Nance, W.E. (2006). Newborn hearing screening–a silent revolution. N. Engl. J. Med. 354, 2151–2164. https://doi.org/10.1056/NEJMra050700.

26. Sloan-Heggen, C.M., Bierer, A.O., Shearer, A.E., Kolbe, D.L., Nishimura, C.J., Frees, K.L., Ephraim, S.S., Shibata, S.B., Booth, K.T., Campbell, C.A., et al. (2016). Comprehensive genetic testing in the clinical evaluation of 1119 patients with hearing loss. Hum. Genet. 135, 441–450. https://doi.org/10.1007/s00439-016-1648-8.

27. Estivill, X., Fortina, P., Surrey, S., Rabionet, R., Melchionda, S., D'Agruma, L., Mansfield, E., Rappaport, E., Govea, N., Milà, M., et al. (1998). Connexin-26 mutations in sporadic and inherited sensorineural deafness. Lancet 351, 394–398. https://doi.org/10.1016/S0140-6736(97)11124-2.

28. Denoyelle, F., Marlin, S., Weil, D., Moatti, L., Chauvin, P., Garabédian, E.N., and Petit, C. (1999). Clinical features of the prevalent form of childhood deafness, DFNB1, due to a connexin-26 gene defect: implications for genetic counselling. Lancet 353, 1298–1303. https://doi.org/10.1016/S0140-6736(98)11071-1.

29. Kelley, P.M., Harris, D.J., Comer, B.C., Askew, J.W., Fowler, T., Smith, S.D., and Kimberling, W.J. (1998). Novel mutations in the connexin 26 gene (GJB2) that cause autosomal recessive (DFNB1) hearing loss. Am. J. Hum. Genet. 62, 792–799. https://doi.org/10.1086/301807.

30. Del Castillo, F.J., and Del Castillo, I. (2017). DFNB1 non-syndromic hearing impairment: diversity of mutations and associated phenotypes. Front. Mol. Neurosci. 10, 428. https://doi.org/10.3389/fnmol.2017.00428.

31. Faridi, R., Tona, R., Brofferio, A., Hoa, M., Olszewski, R., Schrauwen, I., Assir, M.Z.K., Bandesha, A.A., Khan, A.A., Rehman, A.U., et al. (2019). Mutational and phenotypic spectra of KCNE1 deficiency in jervell and lange-nielsen syndrome and romano-ward syndrome. Hum. Mutat. 40, 162–176. https://doi.org/10.1002/humu.23689.

32. Honda, K., Lee, H.J., Griffith, A.J., and Roux, I. (2021). Dissection of the endolymphatic sac from mice. J. Vis. Exp. https://doi.org/10.3791/62375.

33. Honda, K., Kim, S.H., Kelly, M.C., Burns, J.C., Constance, L., Li, X., Zhou, F., Hoa, M., Kelley, M.W., Wangemann, P., et al. (2017). Molecular architecture underlying fluid absorption by the developing inner ear. Elife 6, e26851. https://doi.org/10.7554/eLife.26851.

34. Dahlmann, A., and von Düring, M. (1995). The endolymphatic duct and sac of the rat: a histological, ultrastructural, and immunocytochemical investigation. Cell Tissue Res. 282, 277–289. https://doi.org/10.1007/BF00319118.

35. Crispino, G., Galindo Ramirez, F., Campioni, M., Zorzi, V., Praetorius, M., Di Pasquale, G., Chiorini, J.A., and Mammano, F. (2017). In vivo genetic manipulation of inner ear connexin expression by bovine adeno-associated viral vectors. Sci. Rep. 7, 6567. https://doi.org/10.1038/s41598-017-06759-y.

36. Kim, M.A., Kim, S.H., Ryu, N., Ma, J.H., Kim, Y.R., Jung, J., Hsu, C.J., Choi, J.Y., Lee, K.Y., Wangemann, P., et al. (2019). Gene therapy for hereditary hearing loss by SLC26A4 mutations in mice reveals distinct functional roles of pendrin in normal hearing. Theranostics 9, 7184–7199. https://doi.org/10.7150/thno.38032.

37. Isgrig, K., McDougald, D.S., Zhu, J., Wang, H.J., Bennett, J., and Chien, W.W. (2019). AAV2.7m8 is a powerful viral vector for inner ear gene therapy. Nat. Commun. 10, 427. https://doi.org/10.1038/s41467-018-08243-1.

38. Wangemann, P. (2002). K+ cycling and the endocochlear potential. Hear. Res. 165, 1–9. https://doi.org/10.1016/s0378-5955(02)00279-4.

39. Pickles, J.O.; E.books Corporation (2012). An Introduction to the Physiology of Hearing, Fourth ed. (Emerald Group Pub).

40. Isgrig, K., and Chien, W.W. (2018). Posterior semicircular canal approach for inner ear gene delivery in neonatal mouse. J. Vis. Exp. 56648. https://doi.org/10.3791/56648.

41. Wangemann, P., Liu, J., and Marcus, D.C. (1995). Ion transport mechanisms responsible for K+ secretion and the transepithelial voltage across marginal cells of stria vascularis in vitro. Hear. Res. *84*, 19–29. https://doi.org/10.1016/0378-5955(95)00009-s.

42. Li, Y., Watanabe, K., Fujioka, M., and Ogawa, K. (2017). Characterization of slow-cycling cells in the mouse cochlear lateral wall. PLoS One *12*, e0179293. https://doi.org/10.1371/journal.pone.0179293.

43. Morton, N.E. (1991). Genetic epidemiology of hearing impairment. Ann. N. Y. Acad. Sci. *630*, 16–31.

44. Agrawal, Y., Platz, E.A., and Niparko, J.K. (2008). Prevalence of hearing loss and differences by demographic characteristics among US adults: data from the National Health and Nutrition Examination Survey, 1999-2004. Arch. Intern. Med. *168*, 1522–1530. https://doi.org/10.1001/archinte.168.14.1522.

45. Gates, G.A., and Mills, J.H. (2005). Presbycusis. Lancet *366*, 1111–1120. https://doi.org/10.1016/S0140-6736(05)67423-5.

46. Liu, T., Li, G., Noble, K.V., Li, Y., Barth, J.L., Schulte, B.A., and Lang, H. (2019). Age-dependent alterations of Kir4.1 expression in neural crest-derived cells of the mouse and human cochlea. Neurobiol. Aging *80*, 210–222. https://doi.org/10.1016/j.neurobiolaging.2019.04.009.

47. Everett, L.A., Glaser, B., Beck, J.C., Idol, J.R., Buchs, A., Heyman, M., Adawi, F., Hazani, E., Nassir, E., Baxevanis, A.D., et al. (1997). Pendred syndrome is caused by mutations in a putative sulphate transporter gene (PDS). Nat. Genet. *17*, 411–422. https://doi.org/10.1038/ng1297-411.

48. Ito, T., Li, X., Kurima, K., Choi, B.Y., Wangemann, P., and Griffith, A.J. (2014). Slc26a4-insufficiency causes fluctuating hearing loss and stria vascularis dysfunction. Neurobiol. Dis. *66*, 53–65. https://doi.org/10.1016/j.nbd.2014.02.002.

49. Klein, R.L., Dayton, R.D., Leidenheimer, N.J., Jansen, K., Golde, T.E., and Zweig, R.M. (2006). Efficient neuronal gene transfer with AAV8 leads to neurotoxic levels of tau or green fluorescent proteins. Mol. Ther. *13*, 517–527. https://doi.org/10.1016/j.ymthe.2005.10.008.

50. Niggemann, P., György, B., and Chen, Z.Y. (2020). Genome and base editing for genetic hearing loss. Hear. Res. *394*, 107958. https://doi.org/10.1016/j.heares.2020.107958.

51. Géléoc, G.G.S., and El-Amraoui, A. (2020). Disease mechanisms and gene therapy for Usher syndrome. Hear. Res. *394*, 107932. https://doi.org/10.1016/j.heares.2020.107932.

52. Ramachandran, P.S., Lee, V., Wei, Z., Song, J.Y., Casal, G., Cronin, T., Willett, K., Huckfeldt, R., Morgan, J.I.W., Aleman, T.S., et al. (2017). Evaluation of dose and safety of AAV7m8 and AAV8BP2 in the non-human primate retina. Hum. Gene Ther. *28*, 154–167. https://doi.org/10.1089/hum.2016.111.

53. Taukulis, I.A., Olszewski, R.T., Korrapati, S., Fernandez, K.A., Boger, E.T., Fitzgerald, T.S., Morell, R.J., Cunningham, L.L., and Hoa, M. (2021). Single-cell RNA-seq of cisplatin-treated adult stria vascularis identifies cell type-specific regulatory networks and novel therapeutic gene targets. Front. Mol. Neurosci. *14*, 718241. https://doi.org/10.3389/fnmol.2021.718241.